

15.7 Heterogeneous Integrated CMOS-Graphene Sensor Array for Dopamine Detection

Bayan Nasri, Ting Wu, Abdullah Alharbi, Mayank Gupta, Ramkumar Ranjitkumar, Sunit Sebastian, Yue Wang, Roozbeh Kiani, Davood Shahrjerdi

New York University, Brooklyn, NY

Understanding dopamine (DA) signaling in the brain is essential for advancing our knowledge of pathological disorders such as drug addiction, Parkinson's disease, and schizophrenia. Currently, fast-scan cyclic voltammetry (FSCV) with carbon microfiber (CMF) electrodes is the method of choice in neuroscience labs for monitoring the concentration of phasic (transient) DA release. This method offers sub-second temporal resolution and high specificity because the signal of interest occurs at a known potential. However, existing CMF electrodes are bulky, limiting the spatial resolution to single-site measurements. Further, they are produced through manual processes (e.g. cutting CMFs under optical microscope), thus introducing significant device variability [1]. Lastly, when long probes (3-to-5cm) are used to monitor DA release in deep brain structures of large animals, environmental noise severely diminishes the detection limit [1]. To address these problems, we combine advances in nanofabrication with silicon chip manufacturing to create a heterogeneous integrated CMOS-graphene sensor for accurate measurement of DA with high spatiotemporal resolution (Fig. 15.7.1).

To significantly reduce the environmental noise, it is essential to implement the working electrodes close to the readout system. We achieved this goal with a heterogeneous integration scheme and implementing the electrodes directly on top of the CMOS chip. This was made possible by replacing bulky cylindrical CMF wires with ultra-thin planar multilayer graphene sheets. Integration of the electrodes with the CMOS chip was achieved through post-processing, which involved transfer of the epitaxial graphene film onto the chip, followed by multiple lithographic and metal deposition steps to create miniaturized graphene electrodes and subsequently connect them to their corresponding readout channels (Fig. 15.7.1).

In traditional FSCV, a triangular voltage waveform is applied directly to the working electrode (WE) with respect to a reference electrode (RE). The resulting FSCV signal (I_{FSCV}) consists of two components: (1) a small electrochemical current (I_{DA}) originating from the redox reaction of DA with carbon; (2) a large background current (I_{bg}) due to charge and discharge of the electrical double layer capacitance by the voltage ramp. The peak of I_{DA} during oxidation is proportional to the DA concentration, whereas I_{bg} gives no information about the DA concentration. Further, I_{bg} is much larger than I_{DA} (Fig. 15.7.2), thereby necessitating a readout circuit with large dynamic range and high resolution [2-4]. This imposes significant design challenges for reducing the power consumption and active area. To address this challenge, we take advantage of the high specificity of FSCV and capture the signal at about the redox potentials (which are the regions of interest). Figure 15.7.2 shows the concept and the architecture of our FSCV readout circuit. In our approach, we apply two constant subtraction currents ($I_{sub,p}$ and $I_{sub,n}$) in the positive and negative directions to subtract a large portion of I_{bg} near the regions of interest while maintaining the overall shape of the signal.

Figure 15.7.3 illustrates the transistor-level schematic of the circuit with its timing diagram. We use a three-electrode method to perform FSCV, in which the triangular voltage waveform is applied to a graphene counter electrode (CE) through an integrated counter amplifier circuit. Figure 15.7.3 schematically shows this concept, together with the equivalent circuit model of the reference (RE), CE, and WE electrodes in the solution. Subsequently, the current produced at WE (i.e. $I_{bg}+I_{DA}$) flows into the readout circuit. The amplitude of I_{bg} might vary from a few hundreds of nA to a few μ A, depending on the size of the working electrode and the ramp rate of the input voltage. To support such a broad range of device operation, we implemented a programmable 5b current DAC with a dynamic range of 80nA to 2.56 μ A. Given the small amplitudes of I_{DA} , the current subtraction block should have extremely low noise and low offset error to avoid the degradation or distortion of the input signal. Depending on the polarity of I_{FSCV} , either the $\phi_{s,1}$ switch or the $\phi_{s,2}$ switch connects the proper current source to the input current path at node X. The difference between I_{FSCV} and I_{sub} , I_{sgnl} , flows into a dual-slope ADC, which digitizes the signal. The proper design of switches is critical to prevent the distortion of I_{sgnl} before feeding it into the integrator. The low-noise amplifier

was designed based on the Recycling Folded Cascode (RFC) architecture [5]. The RFC is optimized for noise and consumes $\sim 10\mu$ A. The output of the integrator is then compared with a reference voltage V_{ref} using a dynamic latch comparator with built-in hysteresis for noise rejection. Given the low frequency of the FSCV measurements, we operate the ADC at a sampling frequency of 10kHz.

We fabricated the circuit in a standard 65nm CMOS process. The prototype chip consists of four readout channels. Our strategy for measuring I_{sgnl} in the region of interest allows significant reduction of the channel size ($150\mu\text{m}\times 300\mu\text{m}$), which is adequately small to allow arranging many sensors on a typical neural probe ($<200\mu\text{m}$ wide, 3-to-5cm long). The performance of the readout channel was evaluated by injecting known dc and sinusoidal current signals. Figure 15.7.4 shows the summary of the measurements at 5kHz sampling frequency, indicating a dynamic range of 5nA to 175nA with an SNR of up to 71dB at 150nA. The measured signal resolution is <40 pA. The ADC resolution is an important design parameter, because it determines the minimum detection limit of DA.

We validated the performance of the chip with *in vitro* measurements. A phosphate buffer solution (PBS) and a DA solution in PBS were sequentially introduced into the flow chamber using injection pumps. We measured the sensor response at different input voltage ramp rates of 200V/s, 300V/s, and 400V/s. In FSCV, I_{bg} monotonically increases with increasing the ramp rate, while the device sensitivity also increases noticeably. Given the limited dynamic range of our ADC, it is important to properly determine I_{sub} values. We do this prior to the DA injection. We implemented an algorithm that sequentially varies the DAC code around an initial user-defined I_{sub} at the positive and negative polarities until the ADC measures I_{sgnl} of about 40nA or less at the redox potentials. The initial guess for I_{sub} is made based on the extracted electrical model of the electrodes. In these measurements, we adjusted the $I_{sub,p}$ values (oxidation region) to 670nA, 970nA, and 1.05 μ A for the three ramp rates. To determine the sensor response to DA release, I_{sgnl} is measured before and after introducing DA. The difference of these two currents represents I_{DA} , which is linearly proportional to the DA concentration. Figure 15.7.5 illustrates the results of our *in vitro* measurements for a 2 μ M DA release and the measured sensitivity. We determined the sensitivity from the slope of the fitted line to I_{DA} measured at different DA concentrations. Comparison of the measured sensitivity in Fig. 15.7.5 delineates the advantage of our integrated sensor platform for enhancing the sensitivity with increasing the ramp rate without being limited by I_{bg} . The performance comparison table is shown in Fig. 15.7.6. Figure 15.7.7 illustrates the micrograph of our prototype chip with integrated graphene electrodes.

In conclusion, we introduced and implemented a heterogeneous integrated CMOS-graphene sensor that can enable high-density FSCV measurement of DA. Our sensor design and measurement circuit exceeds the resolution of existing designs and paves the way for precise, multi-site measurement of DA release *in vivo*.

Acknowledgments:

The authors acknowledge United Microelectronics Corporation (UMC) for the support and fabrication of the ASIC. This research used resources of the Center for Functional Nanomaterials, which is a U.S. DOE Office of Science Facility, at Brookhaven National Laboratory under Contract No. DE-SC0012704. RK acknowledges partial financial support by NIMH grant R01MH109180-01.

References:

- [1] E. W. Schluter, et al., "Real-time dopamine measurement in awake monkeys," *PLoS ONE*, vol. 9, no. 6, pp. e98692, June 2014.
- [2] M. Roham, et al., "A Wireless IC for Time-Share Chemical and Electrical Neural Recording," *IEEE J. Solid-State Circuits*, vol. 44, no. 12, pp. 3645 - 3658, Dec. 2009.
- [3] B. Bozorgzadehet, et al., "A Neurochemical Pattern Generator SoC With Switched-Electrode Management for Single-Chip Electrical Stimulation and 9.3 μ W, 78 pArms, 400 V/s FSCV Sensing," *IEEE J. Solid-State Circuits*, vol. 49, no. 4, pp. 881-895, April 2014.
- [4] C. I. Dorta-Quiñones, et al., "A Wireless FSCV Monitoring IC With Analog Background Subtraction and UWB Telemetry," *IEEE Trans. Biomedical Circuits and Systems*, vol. 10, no. 2, pp. 289-299, April 2016.
- [5] R. S. Assaad, et al., "The Recycling Folded Cascode: A General Enhancement of the Folded Cascode Amplifier," *IEEE J. Solid-State Circuits*, vol. 44, no. 9, pp. 2535-2542, Sept. 2009.

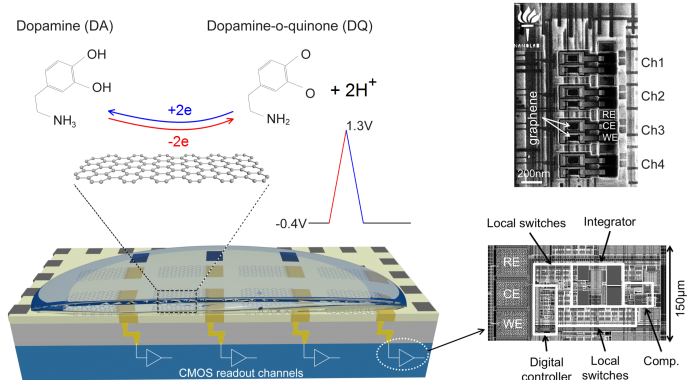


Figure 15.7.1: Extra electrons are produced during FSCV due to redox reaction of DA molecules with carbon atoms. Our prototype integrated CMOS-graphene sensor consists of four channels.

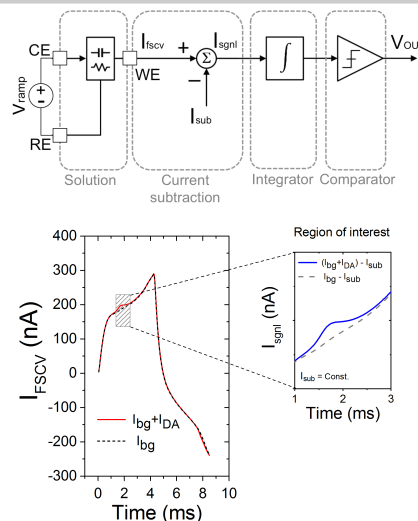


Figure 15.7.2: Architecture of the FSCV readout channel. A large portion of the non-informative I_{bg} is canceled by a constant I_{sub} .

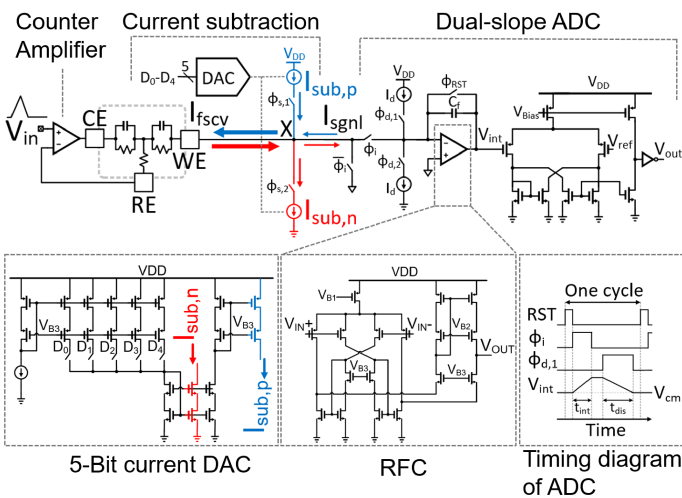


Figure 15.7.3: Transistor-level schematic of the readout circuit with its timing diagram.

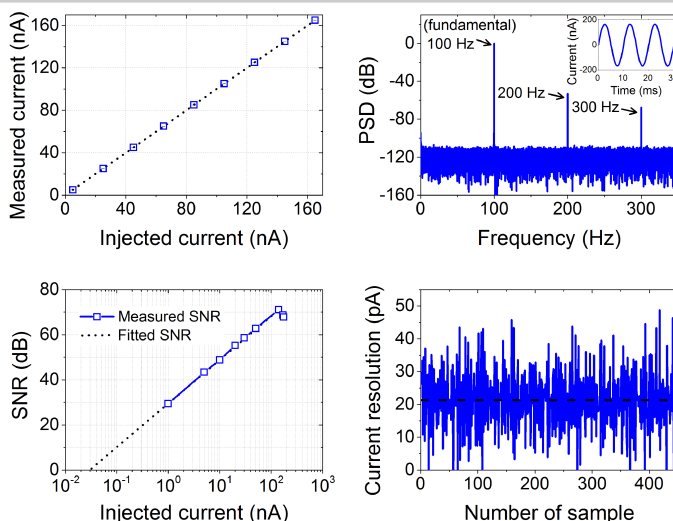


Figure 15.7.4: Performance of the ADC was verified using test dc and sinusoidal current signals with different amplitudes.

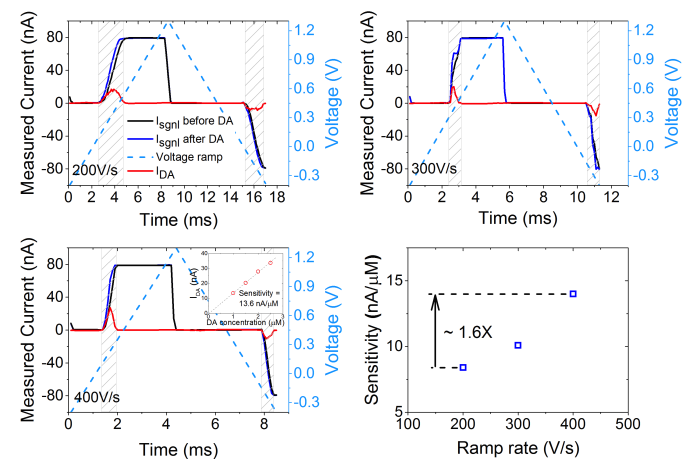


Figure 15.7.5: *In vitro* measurements of $2\mu\text{M}$ DA at different ramp rates. Dashed regions represent the regions of interest around the DA redox potentials. The results confirm the configurability of the circuit for enhancing the sensitivity by increasing the ramp rate.

	This work	[2] 2009 JSSC	[3] 2014 JSSC	[4] 2016 BCAS
Technology	65 nm	0.5 μm	0.35 μm	65 nm
Power supply (V)	1.8	2.5	-0.8, 1.7	1.2, 3.0
Channel size ($\mu\text{m} \times \mu\text{m}$)	150 \times 300	180 \times 1050	113 \times 984	N/A
Power consumption	36 μW	76 μW	9.3 μW	14.4 μW
Input current range	$\pm 2.56 \mu\text{A}$	$\pm 430 \text{ nA}$	$\pm 950 \text{ nA}$	$\pm 430 \text{ nA}$
Resolution	< 50pA	N/A	N/A	50 pA
Dynamic current subtraction	Yes	No	No	Yes
Electrode material/type	Graphene/integrated	CMF/discrete	CMF/discrete	CMF/discrete
Measured ramp rate (V/s)	200, 300, 400 (configurable)	300	400	300

Figure 15.7.6: Comparison with previously published works.

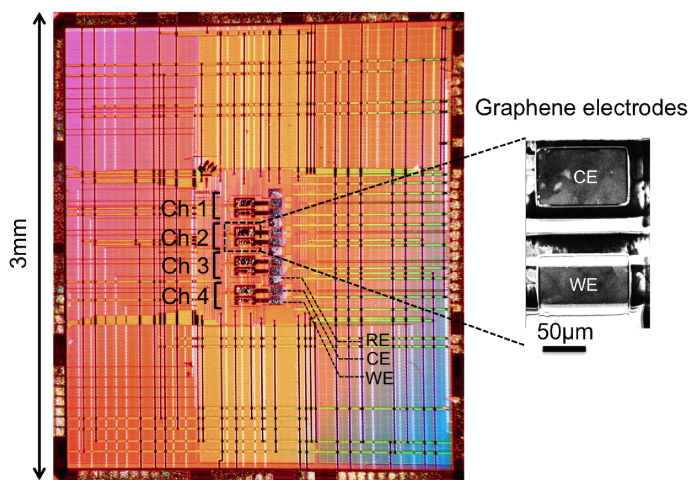


Figure 15.7.7: Micrograph of the CMOS-graphene prototype chip. SEM image of the graphene working and counter electrodes. The size of the CMOS readout channels is $150\mu\text{m}\times 300\mu\text{m}$.